Entropy and dynamics of water in hydration layers of a bilayer

Ananya Debnath, Biswaroop Mukherjee, K. G. Ayappa, Prabal K. Maiti, and Shiang-Tai Lin

Citation: The Journal of Chemical Physics **133**, 174704 (2010); doi: 10.1063/1.3494115
View online: http://dx.doi.org/10.1063/1.3494115
View Table of Contents: http://scitation.aip.org/content/aip/journal/jcp/133/17?ver=pdfcov
Published by the AIP Publishing

Entropy and dynamics of water in hydration layers of a bilayer

Ananya Debnath,[1] Biswaroop Mukherjee,[2] K. G. Ayappa,[1] Prabal K. Maiti,[2,a)] and Shiang-Tai Lin[3]
[1]*Department of Chemical Engineering, Indian Institute of Science, Bangalore 560012, India*
[2]*Department of Physics, Centre for Condensed Matter Theory, Indian Institute of Science, Bangalore 560012, India*
[3]*Department of Chemical Engineering, National Taiwan University, Taipei 10617, Taiwan*

(Received 18 May 2010; accepted 7 September 2010; published online 4 November 2010)

We compute the entropy and transport properties of water in the hydration layer of dipalmitoylphosphatidylcholine bilayer by using a recently developed theoretical scheme [two-phase thermodynamic model, termed as 2PT method; S.-T. Lin *et al.*, J. Chem. Phys. **119**, 11792 (2003)] based on the translational and rotational velocity autocorrelation functions and their power spectra. The weights of translational and rotational power spectra shift from higher to lower frequency as one goes from the bilayer interface to the bulk. Water molecules near the bilayer head groups have substantially lower entropy (48.36 J/mol/K) than water molecules in the intermediate region (51.36 J/mol/K), which have again lower entropy than the molecules (60.52 J/mol/K) in bulk. Thus, the entropic contribution to the free energy change ($T\Delta S$) of transferring an interface water molecule to the bulk is 3.65 kJ/mol and of transferring intermediate water to the bulk is 2.75 kJ/mol at 300 K, which is to be compared with 6.03 kJ/mol for melting of ice at 273 K. The translational diffusion of water in the vicinity of the head groups is found to be in a subdiffusive regime and the rotational diffusion constant increases going away from the interface. This behavior is supported by the slower reorientational relaxation of the dipole vector and OH bond vector of interfacial water. The ratio of reorientational relaxation time for Legendre polynomials of order 1 and 2 is approximately 2 for interface, intermediate, and bulk water, indicating the presence of jump dynamics in these water molecules. © *2010 American Institute of Physics*. [doi:10.1063/1.3494115]

I. INTRODUCTION

Water is a universal solvent for biologically active molecules and plays a crucial role in the formation of self-assembled structures such as reverse micelles, vesicles, and membranes. Membranes form the boundary of living cells and regulate transport in and out of the cell by providing a dynamic interface between the cellular constituents and the extracellular environment. The basic structure of the biological membrane is the lipid bilayer and the interactions between the constituent lipid molecules and water play a major role in the functioning of the membrane, stability of the bilayer, water permeation, and fusion-related repulsive forces between bilayers.[1,2] The presence of the heterogeneous surface of the lipid bilayer can greatly magnify the anomalous properties of water; one such property is the enhanced proton transport along the membrane surface.[3,4] Although the structure and dynamics of water in the vicinity of biomolecules have been investigated for several years, the problem still poses many open questions.[5] In this paper, we concentrate on both the dynamics and thermodynamics of water near the membrane at the molecular scale with special emphasis on the entropy of water in the hydration layer.

Water molecules in the hydration layer of biomolecules play a major role in biomolecular functionalities such as intercalation, enzyme catalysis, and molecular recognition.[6–8] There are a number of investigations of the structure and dynamics of water confined in the vicinity of lipid bilayers and some recent reviews address this subject.[9,10] There have been several reports using IR, nuclear magnetic resonance (NMR), electrical conductivity, and elastic incoherent neutron scattering (EINS) on the interaction between the bilayer head group and water in their immediate vicinity.[11–13] At low hydration, the fourier transform (FT)-IR spectra on the oxygen-deuterium bond (OD) stretch of deuterated water (HOD) molecules in bilayer show that the frequency is redshifted compared to the spectrum of bulk water. The redshift in the absorption spectrum is opposite to the blueshift observed in reverse micelles and Nafion membranes.[11,14,15] Recent ultrafast IR polarization selective pump-probe experiments[11] indicate two major classes of water in the interfacial region of the lipid bilayer. One type of water is classified as a clathrate-like water cluster near the hydrophobic choline group and the other is proposed to be related to the hydration of water molecules mainly associated with the phosphate group. The orientational relaxation from the anisotropic decay is biexponential; the fast component is attributed to small orientational fluctuations which are insensitive to the level of hydration and the slow component is a measure of complete orientational randomization of the hydrogen bond rearrangement, explained in terms of a jump reorientation model.[11]

Molecular dynamics studies on lipid bilayers have also shown the presence of clathrate-like shells at the choline

a)Author to whom correspondence should be addressed. Electronic mail: maiti@physics.iisc.ernet.in. FAX: (091)80-2360-2602.

head group of the bilayer.[16,17] The water molecules that are hydrogen bonded to each other and the double bonded oxygen atoms of phosphate groups exhibit a greater propensity to form hydrogen bonds with two water molecules.[16,18] Molecular dynamics simulations for dimyristoylphosphatidylcholine (DMPC) bilayers attribute four hydrogen bonds to the nonester phosphate oxygens and 1.0 hydrogen bond to the C═O group. Water bridges between the DMPC molecules were found to play an important role in stabilizing the membrane, with a majority of the water bridges formed between the nonester phosphate oxygens.[17] The average lifetime of these water bridges was found to be about 50 ps. In comparison, the lifetime of charge pairs formed between the phosphate and choline groups possess a lifetime of about 150 ps, while the lifetime of DMPC-DMPC pairs can range from 0.7–1.5 ns.[4] Molecular dynamics simulations for 1-palmitoyl-2-oleoyl-phosphatidylcholine (POPC) bilayers[19] reveal that water diffusion parallel to the bilayer plane was slower than diffusion perpendicular to the plane. Reorientational correlation times were significantly higher (320 ps) for water hydrogen bonded to the carbonyl groups when compared with water hydrogen bonded to the phosphate (157 ps) and choline (130 ps) groups. In a molecular dynamics study by Bhide and Berkowitz,[20] the time scale of dipole reorientational decay of the interior water near the vicinity of the dioleoylphosphatidylcholine (DOPC) carbonyl group is on the order of a few tens of picoseconds. To understand the effect of head group motion on the water dynamics, correlation functions have been computed for flexible as well as the frozen lipids and the decay of water in the flexible lipid was found to slow down by a factor of 100–200 times when compared to bulk water. On the other hand, when the lipid is frozen, water relaxation is slowed down by a factor of 30–40 times, indicating coupled motion of the lipid head groups and water. A recent molecular dynamics simulation reports a reduction in orientational relaxation time as the hydration level near bilayer is reduced.[21] This is consistent with experimental data on the same system.[11]

Although structural and dynamical aspects of interfacial water at the bilayer have been widely investigated, for a wide variety of lipid systems, the thermodynamic properties have not received much attention.[10] To our knowledge, water dynamics has not been investigated for the dipalmitoylphosphatidylcholine (DPPC) bilayer which is the focus of the present study. In this paper, we focus on calculating thermodynamic quantities, such as the entropy, in conjunction with several dynamical quantities, such as the survival probability of water molecules in various regions of space, velocity autocorrelation functions (both translational and reorientational), corresponding power spectra, and the translational mean-squared displacements. We also calculate the reorientational correlation functions and the reorientational mean-squared displacements to form a comprehensive picture of all the dynamical processes involved.

There are several theoretical models such as linear response theory, linear interaction energy, and protein dipole Langevin dipoles, which are used to qualitatively explore the thermodynamic properties of surface water.[22–25] However, these methods do not include the contribution of translational entropy to the total hydration entropy. The molecular dynamics study of water in the major and minor grooves of DNA has been recently carried out using a recently developed two-phase thermodynamic model (referred to as the 2PT method) to calculate entropy.[26] The 2PT method, originally developed by Lin *et al.*[27] and applied to argon at different temperatures and densities, showed excellent agreement with entropies evaluated using an equation of state. The same method has been successfully applied to calculate the entropy of bulk water,[28] water in different regions of dendrimers,[29] and entropy of the DNA-dendrimer complex.[30] The value of bulk water entropy obtained from the 2PT method compares very well with other methods based on finite differences,[31] cell theory,[32,33] and pair correlation functions.[34,35] Since the 2PT method has been quite successful in predicting the entropy of argon, liquid water, water near dendrimers, and DNA, we demonstrate the versatility of the same method on a more complex system such as the water-lipid bilayer system investigated in the present paper.

In the present paper, we focus on evaluating the entropy as well as the translational and rotational dynamics of water molecules in different layers adjacent to the DPPC bilayer. In order to identify the extent of heterogeneity at the water-lipid interface, we analyze the properties of water in three different groups identified by their proximity to the phosphate group. This gives rise to three categories of water, namely, interface, intermediate, and bulk. We point out that the definition of water groups is slightly different from those used in earlier works.[19–21,36,37] In addition to the reorientational correlation functions, we compute the survival probabilities and the translational and rotational autocorrelation functions in the different water regimes and their respective power spectra, and analyze rotational and translational diffusion. Additionally, we also evaluate the entropy for the different water layers where contributions from the rotational, vibrational, and translational degrees of freedom to the total entropy are computed. We have also calculated the fluidicity factor of the water in these layers. The organization of the remainder of the paper is as follows: First we describe the details of the simulation method. In Sec. III we discuss our results for the survival probabilities, residence times, and dynamic and thermodynamic properties of water based on the different definitions of water regimes. A summary and conclusions are presented in Sec. IV.

II. SIMULATION DETAILS

Simulations are carried out for bilayers made up of 128 DPPC molecules with 3655 water molecules. This corresponds to a fully hydrated bilayer with a *d*-spacing of 6.43 nm. The chemical formula of single DPPC molecule is shown in Fig. 1. The initial structure of lipid bilayer is taken from the previous work of Tieleman.[38] The simulation box length is 6.41 nm along the x and y directions and 6.43 nm along the z direction. The force-field parameters are obtained using GROMOS-87[39] with the rigid simple point charge (SPC) model for water.[40,41]

An NVT simulation is initially carried out for 3 ns with a time step of 1 fs at 300 K. The Berendsen temperature

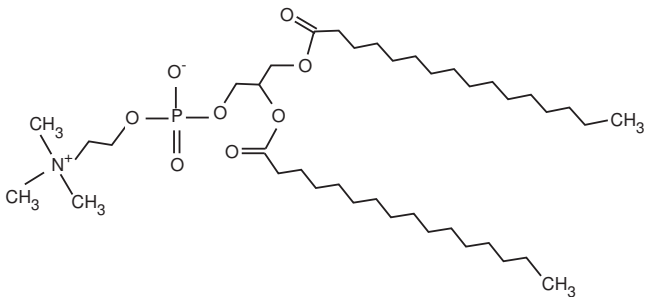

FIG. 1. Chemical formula of DPPC.

coupling method[42] is used with a coupling constant of 1 ps. Coulombic and van der Waals interactions were cut-off at 1.0 nm. Long-range electrostatic interactions were corrected with the particle-mesh Ewald method with a 4.0 nm grid size. Periodic boundary conditions were applied in all three directions and trajectories were collected every 2 ps. Energy, temperature, and pressure are found to be constant with time confirming equilibration. Next, five sets of trajectories of 40 ps duration are simulated and trajectories are collected every 4 fs. As observed earlier by Lin *et al.*,[27] a time scale of 20 ps is sufficient to obtain accurate thermodynamic properties. All simulations are performed with GROMACS 3.3.1.[43,44]

Simulations were also carried out by adding extra water along the z direction to check the effect of hydration levels on the thermodynamic properties. In this case, we have 8663 water molecules in the system. The simulation box length was 6.4 nm along the x and y directions and 10.08 nm along the z direction.

III. RESULTS AND DISCUSSIONS

A. Definition of water regimes

We define three classes of water depending on the value of the z coordinates of the oxygen atoms of the water molecules near the head group-water region of the bilayer. First we compute the layer density profiles of the system as shown in Fig. 2. The different layers of water are based on the value of the z coordinates (perpendicular to the bilayer plane) of the water oxygen molecules. We define water molecules

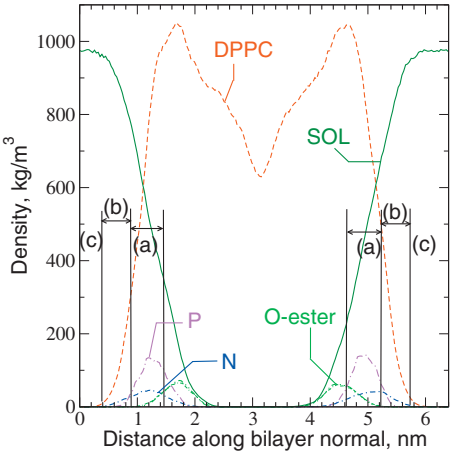

FIG. 2. Density distributions illustrating the (a) interface, (b) intermediate, and (c) bulk water regimes.

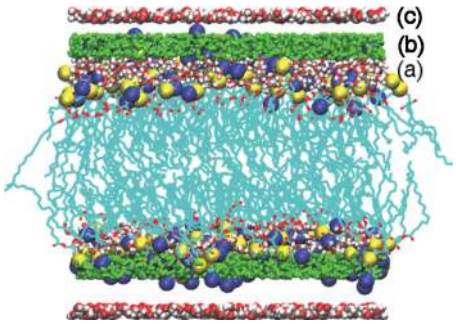

FIG. 3. Equilibrated DPPC bilayer illustrating the three layers of water used in the analysis of dynamical and thermodynamical properties. Color code: (a) red and white liporice: interface water, (b) green: intermediate water, (c) red and white VDW: bulk water, blue: N head, yellow: P head, cyan: carbon, red spot: oxygen ester. For the sake of clarity, an empty space is kept between intermediate and bulk water.

whose oxygen z coordinates remain continuously within ± 3 Å from the phosphorous atom peak positions as interface water. The water molecules which reside continuously within 3–8 Å from the head group (nitrogen peak) position are labeled as intermediate and the molecules which reside continuously above 15 Å away from the head group peak are defined as bulk water. The three different water layers based on the above criterion are illustrated in Fig. 3. From the density distributions, water in the interface region is associated with both the nitrogen of the choline group as well as the phosphorous atom. Although the carbonyl groups are also in the same region, they are located toward the hydrophobic core of the bilayer where the water density is low. Water in the intermediate layer consists of water that has greater association with the methyl groups of choline. The pair correlation functions with the oxygen of the water molecule, $P—O_w$ and $N—O_w$, are illustrated in Fig. 4. This indicates that the interfacial water consists of water around the first and part of the second hydration shell of the phosphorous atom and the first shell of water around the nitrogen atom. We assign a tag 1 to the molecule if it is found to reside in a given layer at a given time step. If the molecule is outside the given layer at any given time step, we assign the tag as 0. Only molecules that reside continuously in a given layer for 40 ps are listed and their thermodynamic and dynamical properties are evaluated.

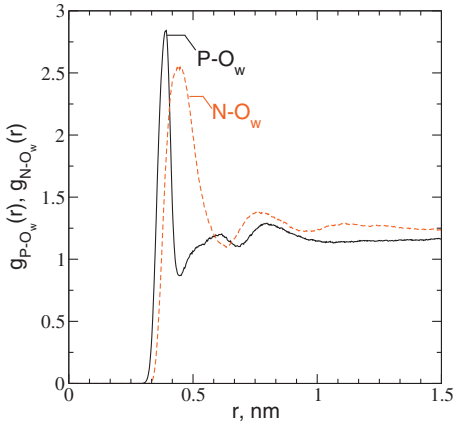

FIG. 4. Radial distribution functions of $g_{P—O_w}(r)$ and $g_{N—O_w}(r)$ illustrating the hydration shells for phosphorus (P) and nitrogen (N), respectively.

B. Survival probability and residence time

An important quantity characterizing the relaxation dynamics of water is the survival probability, which governs the probability of water molecules residing in a given layer. We define $P_i^d(t)$ as the probability (either 0 or 1) of finding the i^{th} water molecule inside layer d (d=interface, intermediate, bulk) at time t and calculate the survival probability $S(t)$ using

$$S(t) = \sum_{i=1}^{N} \left\langle \prod_{t_k=t_0}^{t_0+t} P_i^d(t_k) \right\rangle. \quad (1)$$

This gives the probability that a water molecule resides continuously in layer d for a duration of time t. The summation over i runs over all N water molecules in that layer and the angular bracket denotes the average over time origin t_0. The survival probability is normalized by dividing $S(t)$ of Eq. (1) by $S(0)$, i.e., survival probability at time $t=0$.

We evaluate the survival probabilities for two time windows. The short time window had a duration of 40 ps (sampling frequency of 1 fs) and the long time window the duration was 1 ns (sampling frequency of 2 ps). To quantify the characteristic relaxation times, we fit the normalized survival probability, i.e., $S(t)/S(0)$, to a biexponential function as follows:

$$\frac{S(t)}{S(0)} = A_f \exp\left(-\frac{t}{\tau_f}\right) + A_s \exp\left(-\frac{t}{\tau_s}\right) + y_0. \quad (2)$$

The time evolution of the normalized survival probability for different layers is shown in Fig. 5 for the 40 ps window. The corresponding residence times which are given in Table I reveal two different time scales. Generally, water relaxation has a fast component described by τ_f at a time scale below 2 ps and a slow component described by τ_s at a time scale above 2 ps. For interface water, τ_f is 1.4 ± 0.18 ps and τ_s is 19.26 ± 2.2 ps, whereas τ_f for intermediate water is 1.19 ± 0.4 ps and τ_s is 11.7 ± 1.8 ps. For bulk water τ_f is 0.30 ± 0.03 ps and $\tau_s = 1.96 \pm 0.03$ ps.

The survival probabilities for the long time window of 1 ns are shown in Fig. 6 and the corresponding relaxation times are given in Table II. The results indicate that all the molecules in the interface layer exit within 600 ps. The value of τ_f is 18.04 ± 1.8 ps and τ_s is 102.9 ± 8.79 ps for the interface water, whereas the corresponding values are 8.18 ± 2.4 and 27.6 ± 5.0 ps for the intermediate water layer.

The fast relaxation (τ_s) from the 1 ns analysis corresponds to the slow relaxation (τ_f) from the 40 ps analysis. These times (as listed in Tables I and II) are well within statistical deviations. It should be noted that there are three types of relaxations: a fast relaxation within 2 ps (local vibration), an intermediate relaxation in the range of 10 ps (reflecting the domain environment/confinement), and a long relaxation of 100 ps (residence time). The fast relaxation is common and similar in all the regimes, which corresponds to the time scale of the vibration in a temporary cage formed by the neighboring molecules. The fast relaxation mode (τ_f) increases from 0.3 ps for bulk water to 1.19 ps for intermediate water to 1.4 ps for interface water (shown in Table I), indicating a drastic slowing down of water crossing or vibrating near the bilayer head groups. The different τ_f for different layers is a strong indication of a very distinct environment near the bilayer head group. The slow mode of the relaxation time also increases from 1.96 ps for bulk water to 11.7 ps for intermediate water and 19.26 ps for interface water. For a given time window, the differences reflect the level of heterogeneity in the vicinity of the bilayer. Since the interface water is expected to be dominated by water that is hydrogen

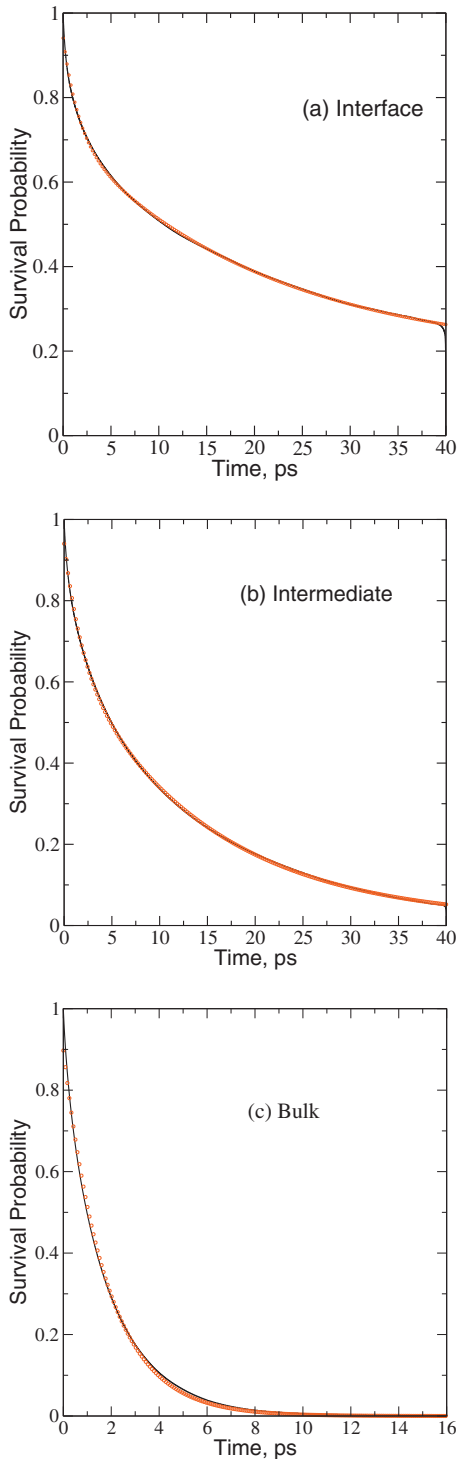

FIG. 5. Survival probability of water in the three different layers of the bilayer (black solid line) evaluated for a duration of 40 ps. The red circles show the fitted data. The residence times obtained from the data fitted to a biexponential [Eq. (2)] for (a), (b) and (c) are shown in Table I.

TABLE I. Residence times for water in three different hydration layers of the bilayer (Fig. 3) analyzed over a 40 ps time window. The residence time increases for both the slow and fast modes from bulk water to intermediate water to interface water. Correlation coefficients for all the cases are >0.99.

System	A_f	τ_f (ps)	A_s	τ_s (ps)
Interface	0.22 ± 0.01	1.4 ± 0.18	0.53 ± 0.03	19.26 ± 2.2
Intermediate	$0.22 \pm .03$	1.19 ± 0.4	0.69 ± 0.02	11.7 ± 1.8
Bulk	0.17 ± 0.01	0.30 ± 0.03	0.82 ± 0.01	1.96 ± 0.03

bonded with the phosphatic group and the water bridges therein, it is likely that the smaller time scale of about 20 ps is related to the average lifetime of the water bridges near the phosphatic group, which have been reported to lie between 30 and 70 ps for POPC lipids.[19] The relaxation time constants for intermediate water indicate a more loosely bound environment associated with the choline groups where clathrate-like water structures have been proposed.[11,45]

Since the survival probabilities have fully decayed to zero, the slow component τ_s is a measure of residence time of water molecules within a specific layer. Though the relaxation time depends on the volume and surface area of different layers, the comparison of corresponding results provide insight into the differences between the dynamically distinct environments in the three layers.

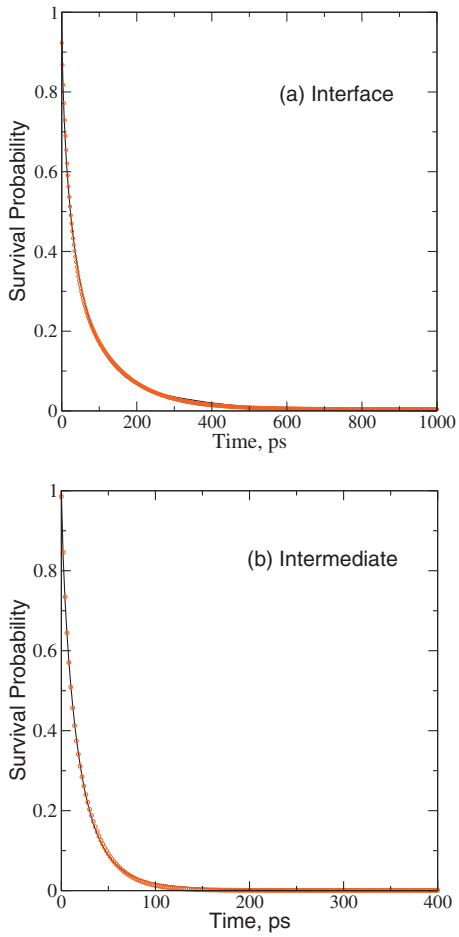

FIG. 6. Survival probability of water in two different layers of the bilayer (black solid line) evaluated for a duration of 1 ns. The red circles show the fitted data. The residence times obtained from the data fitted to a biexponential [Eq. (2)] are shown in Table II.

TABLE II. Residence times for water in three different hydration layers of the bilayer analyzed over a 1 ns window. The residence time increases for both slow and fast modes from bulk water to intermediate to interface water. Correlation coefficients for all the cases are >0.99.

System	A_f	τ_f (ps)	A_s	τ_s (ps)
Interface	0.45 ± 0.01	18 ± 1.8	0.47 ± 0.06	102.9 ± 8.8
Intermediate	0.37 ± 0.06	8.18 ± 2.4	0.59 ± 0.09	27.6 ± 5.0

C. Dynamical properties of water

To detect the changes in the dynamical signatures of water in different layers, we compute the translational and rotational velocity autocorrelation functions (VACFs), as well as their power spectra or density of states (DOS) which are Fourier transforms of the corresponding VACFs. The power spectrum $g(\nu)$ is related to the autocorrelation function $C(t)$ through the Fourier transform

$$g(\nu) = \frac{2}{kT} \lim_{\tau \to \infty} \int_{-\tau}^{\tau} C(t) e^{-2\pi i \nu t} dt. \tag{3}$$

If $C(t)$ is replaced by the mass weighted VACF, which we denote as $C_T(t)$, obtained using the center of mass velocity, $v_i(t)$ of water molecules, then the translational power spectrum $g^T(\nu)$ is obtained. If $C(t)$ is the moment of inertia weighted angular VACF, i.e., $C_R(t)$, then the rotational power spectrum $g^R(\nu)$ is obtained. The molecular center of mass weighted VACF is given by

$$C_T(t) = \sum_{i=1}^{n} m_i \langle v_i^{CM}(t) \, . \, v_i^{CM}(0) \rangle, \tag{4}$$

where m_i is the mass of ith molecule and n is the number of molecules included in the summation. Similarly, the moment of inertia weighted angular VACF is given by

$$C_R(t) = \sum_{j=1}^{3} C_{Rj}(t) = \sum_{j=1}^{3} \sum_{i=1}^{n} I_{ij} \langle \omega_{ij}^{CM}(t) \omega_{ij}^{CM}(0) \rangle, \tag{5}$$

where I_{ij} and ω_{ij} are the jth principle moment of inertia and angular velocity of water molecule i. The integral $g^T(\nu)$ or $g^R(\nu)$ over the whole frequency range (ν=0 to ∞) yields the total degrees of freedom $3n$ of the system, where n is the number of molecules used in the summation of respective autocorrelation functions in Eqs. (4) and (5). n is determined from the list of the molecules which reside continuously in different layers.

The translational and rotational diffusion constants are obtained from corresponding zero frequency density of states, $g_T(\nu=0)$ or $g_R(\nu=0)$, using

$$D_T = \frac{kTg^T(\nu=0)}{12mn} \tag{6}$$

and

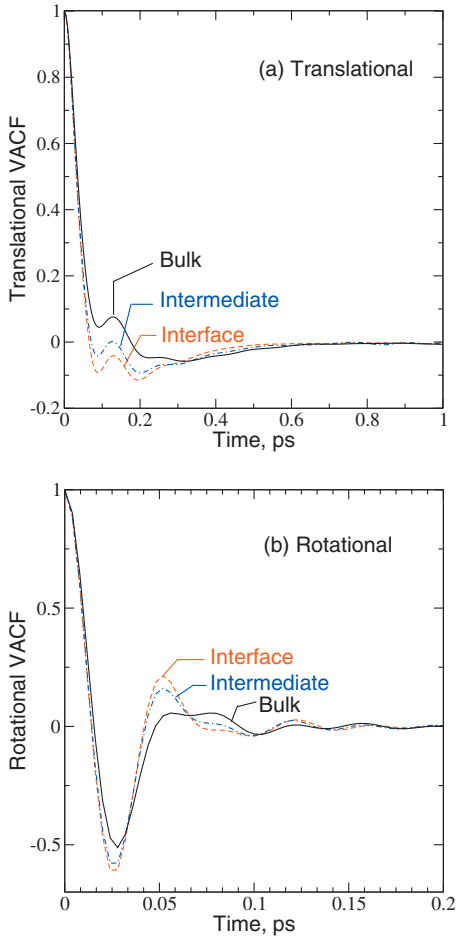

FIG. 7. (a) Translational and (b) rotational velocity autocorrelation functions of water molecules for the three hydration layers.

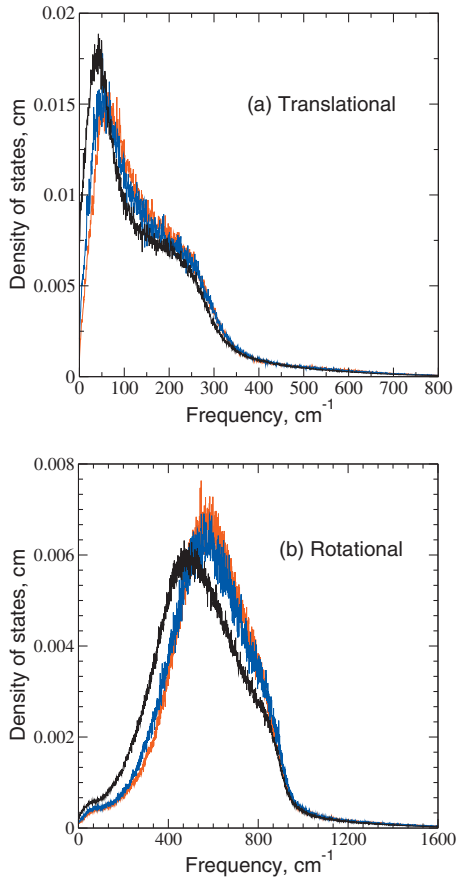

FIG. 8. Averaged (a) translational and (b) rotational power spectra of water molecules. Color code: black: bulk water, blue: intermediate water, red: interface water.

$$D_R = \frac{kT\Sigma_{j=1}^{3} g_{R_j}(\nu = 0)}{4n\Sigma_{j=1}^{3} I_j}. \tag{7}$$

Since all the spectra are normalized by the number of molecules, the integrated density of states is equal to the translational or rotational degrees of freedom, which is three.

The translational and rotational VACF are shown in Figs. 7(a) and 7(b), respectively. The change in the evolution of the VACF from the interface to bulk can be clearly seen in both the translational and rotational VACF. For the translational VACF, the first difference is the presence of well defined negative minima for VACFs in the intermediate and interface regions, with the depth of the minima as well as the intensity of the oscillations increasing for water in the interface. Negative regions in the VACF are associated with reversals of the particle velocity due to collisions with the surrounding molecules. The deeper negative minima in the intermediate and interface regions reveal the presence of a sterically restricted environment associated with the phosphorous and nitrogen groups of DPPC, respectively. Qualitatively similar trends have been observed for water in the hydration layers of proteins.[46] Despite these deviations, at intermediate times the VACFs corresponding to the different regimes decorrelate within 1 ps. Water in all three regions relax in a similar manner at the very short time scales (<0.01 ps) and this is also revealed in the similarities between the translational power spectra at high frequencies [Fig. 8(a)]. The corresponding translational power spectra are shown in Fig. 8(a). The first low frequency peak which arises from the forces in the immediate vicinity or first shell neighbors of the water molecule is distinctly blueshifted going from the bulk toward the interface. We observe a blueshift of 22 cm^{-1} in going from bulk to interface water and 15 cm^{-1} from bulk to intermediate water in the librational peak position of translational power spectra, suggesting that water in the interface is the most tightly bound when compared with water in the intermediate or bulk regions. Another interesting observation is the presence of a shoulder at 200 cm^{-1} due to O—O vibration [Fig. 8(a)] for bulk water, which weakens for water toward the interface. The higher value of $g_T(0)$ from interface to bulk indicates the increase in translational mobility going from the interface to bulk.

The rotational VACF also reveal similar qualitative signatures of a highly constrained environment in the interface and intermediate regions. The rotational VACF displays well defined oscillations in the interface and intermediate regions when compared to bulk water. More pronounced blueshifts in the librational peak position of rotational spectra are observed [see Fig. 8(b)] as one goes from bulk to interface water (by 81 cm^{-1}) and from bulk to intermediate water (by 54 cm^{-1}). Similar to the translational DOS at zero frequency, the rotational DOS at zero frequency $g_R(0)$ also reveals higher rotation diffusion for the bulk water when com-

pared with the intermediate and interface waters. The trends observed in both the translational VACFs and their corresponding power spectra are qualitatively similar to the trends observed in previously reported work on water in the major and minor grooves of DNA.[26]

The translational mean square displacement (MSD) of the water molecules in the three layers are calculated using

$$\langle r^2(t)\rangle = \frac{1}{N}\sum_{i=1}^{N}\langle [r_i(t+t') - r_i(t')]^2\rangle_{t'}, \tag{8}$$

where t is the time difference, t' is the time origin, and N is the number of water molecules. The angular bracket indicates the average over time origins. As the water molecules will exchange their coordinates among three layers with time, we first calculate the number of water molecules which continuously reside in a specific layer for the total simulation time. The number of time origins, as well as the number of water molecules available for averaging in each layer, decrease as one goes to longer time differences t due to the finite life time in each layer. In order to improve the statistics, the reported MSDs are averaged over five independent data sets. At the longest time differences for which the MSD has been reported in this work, the numbers of molecules in the interface, intermediate, and bulk regions are approximately 100, 40, and 200, respectively. The MSD plots for the three layers in different directions are shown in Fig. 9. The fit of the plots with a function At^{α} indicates that the translational diffusion for interface water is slower than the intermediate water, which is again slower than the bulk water. The fitted values show that initially in the subpicosecond timescale (within 40 fs) water molecules in all the three layers exhibit ballistic behavior (value of α is equal to 2). At longer times, within 5–6 ps, water molecules are in the diffusive regime for bulk water, but in subdiffusive regimes for intermediate and interface water (Table III). The diffusion constant for the bulk water in this region is 4.11×10^{-5} cm^2/s which is similar to the reported values of the self-diffusion constant for SPC water $3.6-5.2\times10^{-5}$ cm^2/s.[41] It is critical to determine the exponent of the temporal scaling of the MSD (particularly for short time windows) before one extracts a diffusion coefficient. Since water exhibits subdiffusive behavior in the intermediate and interface layers, we did not attempt to extract a diffusion constant in these layers.

To understand the influence of the lipid head groups on the orientational behavior, we have calculated the reorientational correlation function for the water molecules that continuously reside in three layers. Traditionally, the Debye model has been used to understand the reorientational relaxation of water. This picture assumes that the reorientation proceeds by a multitude of small angular steps. Recently, this traditional picture has been significantly amended by the results obtained using MD simulations,[47–50] which reveals contrary to the long standing belief that water molecules reorient with a combination of diffusion and large amplitude angular jumps. As a result this process is nondiffusive. Several other investigations have tried to understand the reorientational behavior of water molecules under confinement and in the presence of solute molecules in the light of these nondiffusive jump processes. The general consensus that emerges is that these angular jumps are a very generic feature of a molecule such as water. The presence of confinement, in most cases, primarily alters the jump rates (not the mechanism) depending on the strength of interaction between water and its immediate neighborhood.[21,51–58]

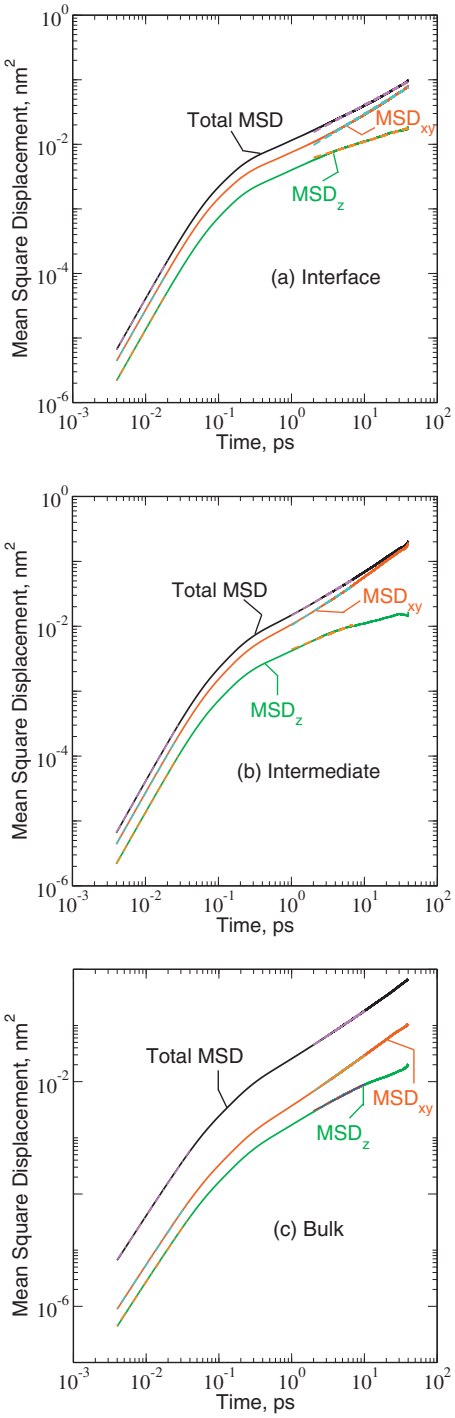

FIG. 9. Mean square displacement for water in three layers. The dotted lines show the fittings for initial subpicosecond region (within 40 fs) and for picosecond region (within 1–6 ps).

To characterize the reorientational relaxation of the dipole moment vector, one calculates the lth order correlation function given by

TABLE III. The values of α from fitting of translational mean square displacement of water with function At^{α} in three different layers for the ps region (within 1–6 ps). This shows a diffusive region for bulk layers, whereas subdiffusive regions for intermediate and interface layer. Correlation coefficients for all the cases are >0.99.

Layers	MSD_{xy}	MSD_z	MSD_{tot}
Interface	0.6	0.4	0.6
Intermediate	0.7	0.7	0.7
Bulk	0.9	0.9	0.9

where P_l is the lth order Legendre polynomial. As the reorientational correlation function of dipole moment vector can be probed experimentally with NMR, IR, fluorescence depolarization, and the optical Kerr effect,[59–61] we first consider the dipole moment autocorrelation functions calculated for the first order Legendre polynomial $C_{\mu}^{1}(t)$ and for the second order Legendre polynomial $C_{\mu}^{2}(t)$ using Eq. (9), with $\mathbf{e}_i^{\alpha}(t)$ as the dipole moment vector. Later we calculate the OH bond vector correlation function for $l=1$ and $l=2$ with $\mathbf{e}_i^{\alpha}(t)$ as the OH bond vector and show that the behavior is qualitatively consistent with that of the dipole vector.

The time evolution of the first and second order correlation functions of the dipole vector for interface, intermediate, and bulk water are shown in Figs. 10(a)–10(c), respectively. The figures show that the decay of the correlation function for interface and intermediate water does not reach zero within the sampling time window of 40 ps. The nonzero orientational correlation indicates an orientational preference of the dipole of water in the interface region due to the presence of the zwitterionic lipid head group. The decay for intermediate water molecules are faster compared to that of interface water molecules as the water in this layer are away from the head groups. The correlation of bulk water decays to zero indicating a nondirectional configuration.[47]

The orientational relaxation time is determined by fitting the normalized correlation function to the following function:

$$C_{\mu}^{l}(t) = A_0 \exp\left(-\frac{t}{\tau_0^l}\right) + A_1 \exp\left(-\frac{t}{\tau_1^l}\right) + A_2 \exp\left(-\frac{t}{\tau_2^l}\right) + A_3, \tag{10}$$

where $l=1,2$. This functional form contains an additional constant term A_3 to quantify the orientational preference of the water molecules. As discussed above, the fitted value of the constant term continually decreases as one goes from the interface to the bulk-like water. As the water layer which is 15 Å away from the head group peak is bulk-like, not really bulk water, there seems to be the presence of a very small net polarization (the value of A_3 shown in Table IV is very small and non zero). For bulk water, A_1, A_2, and A_3 reduces to zero. The fitted parameters for all the three different layers are presented in Table V. The three time scales obtained for interface and intermediate layers confirm three different relaxation processes in the system. The three time scales can be ordered as fast (τ_0^l), intermediate (τ_1^l), and slow relaxation (τ_2^l), with $\tau_2^l > \tau_1^l > \tau_0^l$. The fast relaxation occurs on the time scale of a few hundreds of femtoseconds, the τ_1^l occurs on the time scale of 3–12 ps, and the τ_2^l occurs on the time scale of 24–100 ps depending on the specific layer. According to a recent explanation, water molecules near a bilayer or surfactants exhibit three relaxation time scales.[62] The fast relaxation τ_0^l is due to librational motion, the intermediate τ_1^l is explained as the rotational relaxation of restricted motion inside a cone, and τ_2^l, the third relaxation, is the relaxation of the cone.[21,63,64]

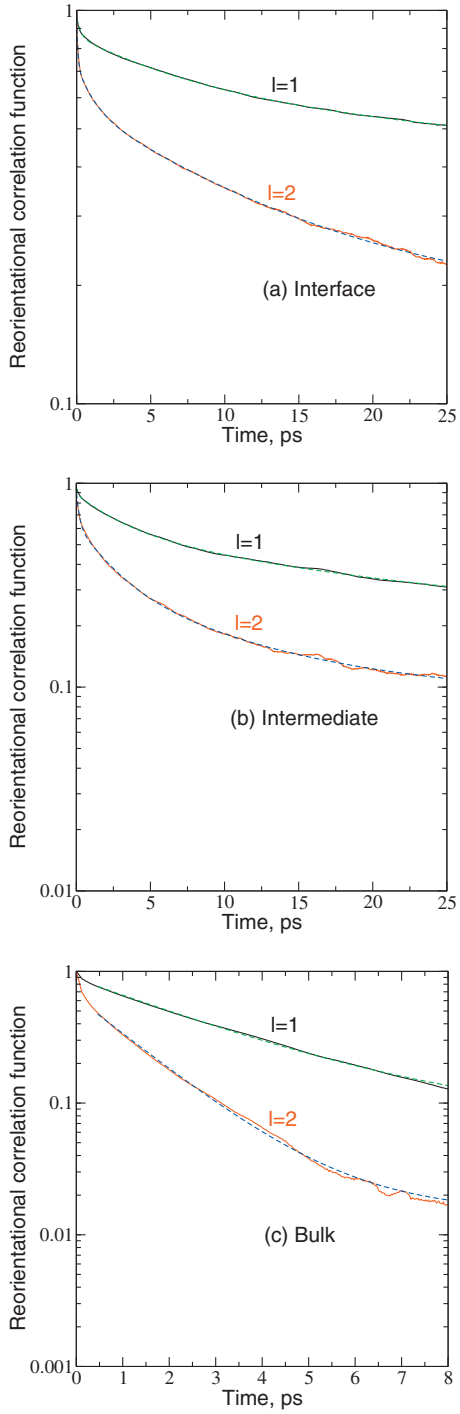

FIG. 10. Reorientational correlation function C_{μ}^{l} for dipole moment vector for $l=1,2$.

We compare the relaxation time of the interface and intermediate water with the corresponding values of the bulk water. As bulk water has only two characteristic relaxation

TABLE IV. Multiexponential fitting parameters for $C_{\mu}^{l}(t)$ calculated for water molecules continuously residing in different regions. For each case, the amplitudes are listed consecutively starting from A_0 and $n=0$. The relaxation time increases from bulk to intermediate to interface water. The ratio of τ_2^1/τ_2^2 is ≈2 for interface, intermediate, and bulk water, indicating the presence of jump dynamics in these regions. The correlation coefficients for all the cases are >0.99.

	Region	Amplitude	τ_n^l (ps)	η_l (ps)
$l=1$		0.1	0.28	
		0.19	6.82	17.33
		0.26	25.02	
		0.41		
	Interface			
$l=2$		0.22	0.1	
		0.16	1.1	9.2
		0.39	12.52	
		0.17		
$l=1$		0.08	0.1	
		0.3	3.1	12.68
		0.38	20.26	
		0.17		
	Intermediate			
$l=2$		0.3	0.18	
		0.3	2.4	5.78
		0.24	10.00	
		0.09		
$l=1$		0.81	3.16	
		0.07		
	Bulk			
$l=2$		0.62	1.53	
		0.01		

TABLE V. Multiexponential fitting parameters for $C_{\mathrm{OH}}^{l}(t)$ calculated for water molecules continuously residing in different regions. The relaxation time increases from bulk to intermediate to interface water. The ratio of τ_2^1/τ_2^2 is 1.2–1.7 for interface, intermediate, and bulk water, indicating the presence of jump dynamics in these regions. The correlation coefficient for all the cases are >0.99.

	Region	Amplitude	τ_n^l (ps)	η_l (ps)
$l=1$		0.07	0.4	
		0.11	3.99	16.97
		0.47	20.01	
		0.30		
	Interface			
$l=2$		0.18	0.12	
		0.16	1.75	12.77
		0.45	16.69	
		0.15		
$l=1$		0.12	0.99	
		0.3	7.23	10.84
		0.34	14.03	
		0.17		
	Intermediate			
$l=2$		0.18	0.41	
		0.24	2.50	
		0.32	9.31	6.39
		0.01		
$l=1$		0.86	3.7	
	Bulk			
$l=2$		0.50	2.12	

times, we compare the longer time decay of bulk water with the average time decay of the longer relaxation time scales for the interface and intermediate water using following function suggested by Bhide and Berkowitz:[20]

$$\eta_l = \frac{A_1}{A_1+A_2}\tau_1^l + \frac{A_2}{A_1+A_2}\tau_2^l. \tag{11}$$

The above definition assumes that the first component (τ_0^l) relaxes much faster than the remaining components and hence does not contribute appreciably to the overall relaxation time as defined above. The average relaxation time constants for interface and intermediate water are listed in Table IV. Compared to the bulk water relaxation time for $l=1$, the relaxation of interfacial water is slowed down by a factor of 8(≈25.02/3.16), whereas the relaxation time for intermediate water is slowed down by a factor of 6(≈20.26/3.16). For $l=2$, interfacial water relaxation is slowed down by a factor of about 86(≈12.52/1.53), whereas the intermediate water relaxation is slowed down by a factor of about 7(≈10.00/1.53). The slowing down of orientational decay is the outcome of the fact that the lipid head groups make hydration shells with surrounding water molecules. This hydration shell rotates slowly compared to bulk water because the translational motion of head groups couple with the orientational relaxation of interface water. This coupling between translational and orientational motion is responsible for the slow relaxation time τ_2^l. This effect is gradually reduced in bulk water. For water inside carbon nanotubes and nanorings, the orientational relaxation slows down compared to the bulk following a similar trend.[65]

If the reorientational relaxation is diffusive, then it can be easily shown that the relaxation time of the lth order Legendre polynomial is given by $(l(l+1)D_R)^{-1}$. Therefore, the ratio of the first two relaxation times, $\tau_2^1/\tau_2^2=3$.[66] From Table IV we show that the ratio is 3.16/1.53=2.06 for bulk water, 20.26/10.00=2.03 for intermediate water, and 25.02/12.52=1.99 for interface water. If η_l yields the average slow relaxation time for interface and intermediate water, then the ratio of η_1/η_2 is 1.88 for interface water and 2.19 for intermediate water. For interface, intermediate and bulk water this ratio deviates significantly from Debye-like behavior, indicating nondiffusive reorientation process.[47,67–69]

Similar reorientational correlations have been calculated for the OH bond vector. The decay of the OH bond reorientational correlation function is shown in Figs. 11(a)–11(c) for

TABLE VI. Rotational diffusion constant rad^2/ps obtained from reorientational mean square displacement decreases from bulk to intermediate to interface water for dipole moment vector, as well as for OH and HH bond vectors. Moreover, the rotational diffusion of dipole moment vector is slower compared to the OH which is again slower than HH bond vectors for all the layers. The correlation coefficient for all the cases are >0.99.

Layers	μ	OH	HH
Interface	1.30	1.48	1.60
Intermediate	1.64	1.86	1.98
Bulk	2.85	3.34	3.66

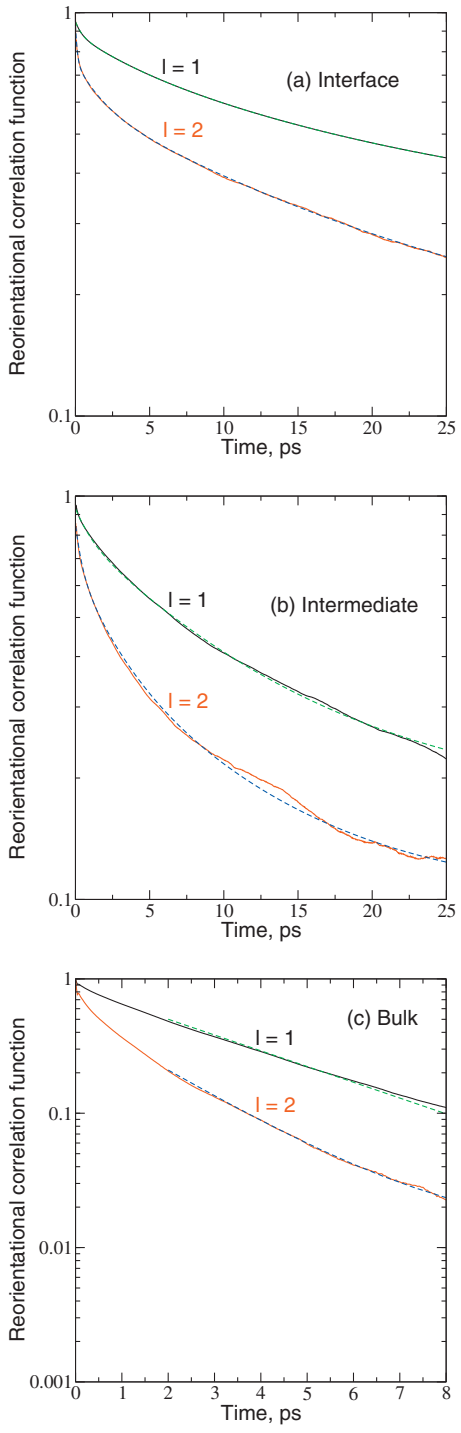

FIG. 11. Reorientational correlation function C_{OH}^{l} for OH bond vector for $l=1,2$.

interface, intermediate and bulk water, respectively. We fit the correlation function with Eq. (10) to extract different relaxation time scales which are presented in Table V. The ratio of τ_2^1/τ_2^2 equals 1.19 for interface water, 1.56 for intermediate water, and 1.74 for bulk water. Hence, we observe that the OH bond vector relaxation follows a trend which is qualitatively similar to that of the dipole moment vector.

One should note that we have calculated reorientational behavior of water molecules at a fixed hydration level (28.55) unlike previous investigations of reorientational dynamics at different hydration levels.[70]

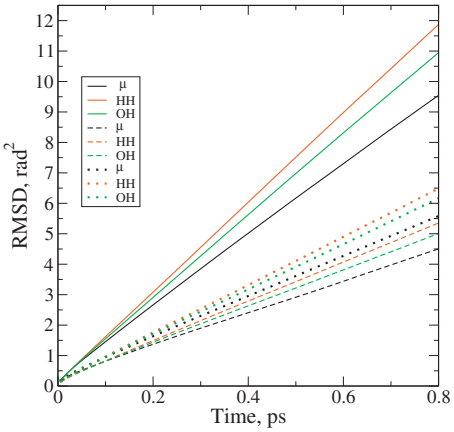

FIG. 12. Rotational mean square displacement, $\Delta\phi^2(t)$, rad^2/ps, for HH, OH, and dipole moment vector for water in three layers. Solid lines: bulk water, dotted lines: intermediate water, and dashed lines: interface water. Color code: black: μ, green: OH, red: HH.

We next evaluate the rotational mean square displacement (RMSD) for water molecules in the three layers. This is a quantity analogous to the translational mean-squared displacement and was originally calculated to characterize the rotational dynamical heterogeneity in glassy water.[71] The rotational angular displacement $[\phi_i(t)-\phi_i(0)]$ is described as the total angular displacement by vectors for discrete time steps of size δt as follows:

$$\phi_i(t) - \phi_i(0) = \sum_{n=0}^{m-1} \delta\phi_i(n\,\delta t, \delta t), \tag{12}$$

where $m=t/\delta t$. A vector, $\mathbf{p}_i(t)$, fixed to the ith molecule at time t spans an angle $\delta\theta=\cos^{-1}[\mathbf{p}_i(t)\cdot\mathbf{p}_i(t+\delta t)]$ and the vector $\delta\phi_i(t,\delta t)$ is defined such that $|\delta\phi_i(t,\delta t)|=\delta\theta$ and with its direction given by $\mathbf{p}_i(t)\times\mathbf{p}_i(t+\delta t)$. The numerical value of δt is taken as 0.4 fs in our calculation. The RMSD is given by

$$\langle\Delta\phi^2(t)\rangle = \frac{1}{N}\sum_i \langle|\phi_i(t) - \phi_i(0)|^2\rangle, \tag{13}$$

where the angular brackets denote the averaging over time origins. The rotational diffusion coefficient is given by

$$D_R = \lim_{t\to\infty}\frac{1}{4t}\langle\Delta\phi^2(t)\rangle. \tag{14}$$

The RMSD for water dipole moment μ, the OH vector, and the HH vector in three layers for short times are shown in Fig. 12. The plot shows that the dipole moment relaxation is the slowest and the HH relaxation is the fastest for water molecules in all three layers which is in agreement with the behavior of reorientational correlation function. Bulk water is found to relax faster in comparison to water in the intermediate and the interface regions. For further confirmation, we calculate rotational diffusion constant for all three layers of water from the slopes of RMSD (shown in Fig. 12). The tabulated rotational diffusion constant in Table VI demonstrates that the rotational diffusion constant for the dipole moment is the slowest and that for HH vector is the fastest for all the three layers. Comparisons of the diffusion constant of dipole moment vector as well as OH and HH vector, for

TABLE VII. Entropy of water in three different hydration layers of the bilayer. $S_{trans}=S_{vib}+S_{conf}$ and $S_{tot}=S_{rot}+S_{trans}$.

Properties	Interface	Intermediate	Bulk
$g_T(\omega=0)$ $(10^{-2}$ cm)	0.09	0.21	0.74
$g_R(\omega=0)$ $(10^{-4}$ cm)	0.93	1.43	1.91
Translational librational peak (cm^{-1})	63.89	57.22	42.22
Rotational librational peak (cm^{-1})	584.44	558.33	503.89
Fluidicity factor (f)	0.08 ± 0.01	0.13 ± 0.06	0.25 ± 0.01
S_{vib} (J/mol/K)	36.62 ± 0.47	35.27 ± 0.54	31.34 ± 1.23
S_{conf} (J/mol/K)	5.87 ± 1.01	9.81 ± 0.89	21.02 ± 1.37
S_{trans} (J/mol/K)	42.49 ± 0.72	45.08 ± 0.53	52.36 ± 0.50
S_{rot} (J/mol/K)	5.87 ± 0.11	6.28 ± 0.29	8.16 ± 0.16
S_{tot} (J/mol/K)	48.36	51.36	60.52

three layers of water, shows that the rotational dynamics is slowest for the interfacial water and fastest for the bulk.

D. Water entropy

We compute entropy of water molecules in each layer using the 2PT model developed by Lin *et al.*[27] The density of states $(g(\nu))$ of the system is partitioned into a gaslike and solidlike component

$$g(\nu)=g^g(\nu)+g^s(\nu), \tag{15}$$

where $g^g(\nu)$ is the gaslike diffusive component and $g^s(\nu)$ is the solidlike component. One can calculate entropy of the system by weighting the individual density of states with proper functions as follows:

$$S=\int_0^\infty g^g(\nu)W_S^g(\nu)+\int_0^\infty g^s(\nu)W_S^s(\nu), \tag{16}$$

where $W_S^s(\nu)$ is the weighting function of a harmonic oscillator assuming each mode in the solid phase is a harmonic oscillator and $W_S^g(\nu)$ is the weighting function of the gas component described by a hard sphere fluid. In Eq. (16), $W_S^s(\nu)$ can be written as

$$W_S^s(\nu)=\frac{\beta\hbar\nu}{\exp(\beta\hbar\nu)-1}-\ln[1-\exp(-\beta\hbar\nu)], \tag{17}$$

where $\beta=1/kT$ and $\hbar=h/2\pi$, where h is the Planck's constant. In Eq. (16),

$$W_S^g(\nu)=\frac{1}{3}\frac{S^{HS}}{k}, \tag{18}$$

where S^{HS} is the hard sphere entropy determined from the Carnahan–Starling equation of state.[72] The entropy obtained from the solidlike component is known as the vibrational entropy and the one obtained from the gaslike component is known as the configurational entropy. Hence, with a knowledge of the density of states, the corresponding entropy contribution can be evaluated.

The gaslike density of states is calculated using the hard sphere diffusive model as

$$g^g(\nu)=g^{HS}(\nu)=\frac{g_0}{1+(g_0\nu/12fN)^2}, \tag{19}$$

where g_0 is $g^T(\nu=0)$ described previously and f is a so called fluidicity factor. $f=1$ describes that the system as a hard sphere gas at the higher temperatures and/or low density limit without a solidlike component and $f=0$ describes the system as a solid in the high density limit without a gaslike component defining f proportional to the diffusivity. Using the self-diffusivity of the system D, determined from Eq. (6), f is written as follows:

$$f=\frac{D(T,\rho)}{D_0^{HS}(T,\rho;\sigma^{HS})}, \tag{20}$$

where D_0^{HS} is the hard sphere diffusivity in the zero pressure limit[73] and σ^{HS} is the hard sphere diameter. In terms of normalized diffusivity Δ, a universal expression for f is obtained as

$$2\Delta^{-9/2}f^{15/2}-6\Delta^{-3}f^5-\Delta^{-3/2}y^{7/2}+6\Delta^{-3/2}f^{5/2}+2f-2=0 \tag{21}$$

and Δ is expressed in terms of g_0 as follows:

$$\Delta(T,\rho,m,g_0)=\frac{2g_0}{9N}\left(\frac{\pi KT}{m}\right)^{1/2}\rho^{1/3}\left(\frac{6}{\pi}\right)^{2/3}. \tag{22}$$

As we know $g^T(0)$ from simulation, Δ is calculated using above equation which is again used to get fluidicity factor from Eq. (21). Knowing g_0 and f, we calculate $g^g(\nu)$ using Eq. (19) and $g^s(0)$ using $g^s(\nu)=g^T(\nu)-g^g(\nu)$.

The values of entropy in different layers are shown in Table VII. We calculate vibrational entropy (S_{vib}) and configurational entropy (S_{conf}) of water molecules in each layer using the equations described above. The values of the vibrational entropy decrease from interface to intermediate and intermediate to bulk. This can be understood by examining the translational librational peak values in Table VII as well as the translational power spectra in Fig. 8(a). The librational peak positions show a blueshift from bulk water to intermediate water to interface water. The power spectra broaden from bulk to intermediate to interface water. As the vibrational entropy is calculated from the area under the curve of the translational power spectra using Eq. (17), the broadening in the power spectra reflects in the increment in vibra-

TABLE VIII. Entropic contribution to the free energy change for some processes.

Process	Temperature (K)	Entropic change, $T\Delta S$ (kJ/mol)
Release of water from interface to bulk	300	3.65 ± 0.18
Release of water from intermediate to bulk	300	2.75 ± 0.16
Melting of ice	273	6.03

tional entropy from bulk water to intermediate to interface water. The configurational entropies S_{conf}, calculated from the gaslike component of density of states, for water in three layers, show the reverse order compared to that of vibrational entropy. This is explained by the increased value of fluidicity factor in Table VII from interface to intermediate to bulk water. The translational as well as rotational entropies increase from interface water to intermediate to bulk, demonstrating the bound nature of water near bilayer head groups. On comparing total entropy of water molecules in different layers, it is clear that water in the interface region are more ordered than the intermediate water, which are more ordered than bulk. The total entropy for bulk-like water away from bilayer from our calculation is 60.52 $JK^{-1}\ mol^{-1}$. Note that in our simulations this bulk-like region of water is small due to the low hydration numbers used in our study. Hence, the density of water in this region is lower than that of bulk water. So we carried out an NVT simulation for 512 bulk SPC water molecules at 298 K and at a density of 1 g/cc for 100 ps. Entropy for bulk water from our simulation is 63.9 $JK^{-1}\ mol^{-1}$, whereas the reported value is $65.10 \pm 3.35\ JK^{-1}\ mol^{-1}$ obtained from a finite difference method.[31]

We compare the entropic change ($T\Delta S$) associated with the process of release of water from interface to bulk and intermediate to bulk with that of the melting of ice in Table VIII, as both involve delocalization of water molecules. At 300 K, the change in entropy due to release of water from interface to bulk is 3.65 kJ/mol and from intermediate to bulk water is 2.75 kJ/mol, whereas the change in entropy due to melting of ice is 6.03 kJ/mol at 273 K. Hence the increase in entropy associated with the transfer of water from the interface and intermediate regions to bulk water is significant when compared to the entropy change due to melting.

To confirm whether the initial 3 ns NVT run was sufficient for equilibrating the system, we performed a 10 ns NVT simulation and the entropy was recalculated. The comparison of the results from these two calculations are shown in Table IX. The result from the 10 ns run did not vary significantly from the 3 ns run.

We also carried out another 10 ns NVT simulation with excess water where the resulting *d*-spacing for the bilayer is 10.08 nm. In our earlier set of simulations the *d*-spacing for the bilayer was 6.43 nm. The results for this larger *d*-spacing calculation are shown in Table X. We do not find any significant difference for the bulk entropy between two different systems.

IV. CONCLUSIONS

We have demonstrated the unusual dynamical and thermodynamical behavior of water in the vicinity of the lipid bilayer. Using a simple criterion based on the water density profile along bilayer normal, water is classified into three layers of water: interface water near bilayer head groups, intermediate water, and far water denoted as bulk. The presence of the head group affects the translational and the reorientational diffusion of the nearby water molecules. The translational diffusion of water in the interface and intermediate layer is significantly slower than that of bulk. The librational motions of interface and intermediate water are more restricted compared to bulk. We have compared the reorientational time correlation functions for the water dipole and HH and OH bond vectors of water in the three layers and found that the interfacial water appears to be significantly different than the water in the bulk. The bound water molecules in the interface exhibit slower relaxation with the longest component around several tens of picoseconds, while the intermediate water molecules show relatively faster relaxation. However, the bulk water molecules exhibit fastest relaxation when compared to the interface or intermediate water.

An important finding of the present work is the difference in the vibrational spectral features of the interfacial water molecules with that of bulk water. We observe a blueshift of 22 cm^{-1} from bulk to interface water and 15 cm^{-1} from bulk to intermediate water in the librational peak position of translational power spectra and 81 cm^{-1} from bulk to interface water and 54 cm^{-1} from bulk to intermediate water in the librational peak position of rotational spectra. This result is consistent with the observations on the relative effects of the interface on translational diffusion of water molecules and their orientational relaxation. The rotational diffusion is also strongly affected by the bilayer head groups. For dipole moments and HH, OH bond vectors, the rotational diffusion is slower near bilayer interface compared to the intermediate

TABLE IX. Comparison of entropy of water in three different hydration layers of the bilayer after 10 and 3 ns equilibration run. $S_{tot}=S_{rot}+S_{trans}$.

	Interface		Intermediate		Bulk	
Properties	10 ns	3 ns	10 ns	3 ns	10 ns	3 ns
S_{trans} (J/mol/K)	41.72 ± 0.33	42.49 ± 0.72	47.91 ± 0.71	45.08 ± 0.53	53.02 ± 0.51	52.36 ± 0.50
S_{rot} (J/mol/K)	5.53 ± 0.09	5.87 ± 0.11	7.17 ± 0.22	6.28 ± 0.29	7.44 ± 1.68	8.16 ± 0.16
S_{tot} (J/mol/K)	47.25	48.36	55.08	51.36	60.46	60.52

TABLE X. Comparison of entropy for bulk water between systems having *d*-spacing of 10.08 and 6.43 nm.

	Bulk	
Properties	*d*-spacing (nm) 10.08	*d*-spacing (nm) 6.43
S_{trans} (J/mol/K)	53.45 ± 0.11	52.36 ± 0.50
S_{rot} (J/mol/K)	7.6 ± 1.4	8.16 ± 0.16
S_{tot} (J/mol/K)	61.05	60.52

which is again slower compared to the bulk. The ratio of reorientational relaxation time for Legendre polynomials 1 and 2 for interface and intermediate water is 2, indicating that the jump dynamics is present in the water in both the layers.

We have calculated the entropy of the water molecules in the interface water near the bilayer head groups, as well as in the intermediate layer and bulk water using the recently developed method by Lin *et al.*[27,29] The present work states that the entropy of interface water is lower than that of intermediate water which is again lower than bulk water. The entropy change due to release of water molecules from interfacial region of bilayer to the intermediate region (3 J/mol/K) and from intermediate to bulk (9.16 J/mol/K) is quite significant compared to the entropy release associated with the melting of ice (22.1 J/mol/K). So water molecules in the interfacial region are ordered compared to those in bulk. This ordering is further confirmed from the slow reorientational relaxation time of the interfacial water compared to intermediate and bulk water. The increased ordering of the water in the solvation shell near lipid head groups might indicate the evidence of theoretical "iceberg" water model[74] which has been recently tested by the mid-IR spectroscopy experiments[75] and has been discussed in detail in the context of the origin of hydrophobic effect.[76]

ACKNOWLEDGMENTS

We would like to thank Procter and Gamble, USA for financial support.

[1] K. Gawrisch, H. C. Gaede, M. Mihailescu, and S. H. White, Eur. Biophys. J. **36**, 281 (2007).
[2] D. E. Metzler, *Biochemistry: The Chemical Reactions of Living Cells*, 2nd ed. (Harcourt/Academic, San Diego, 2001).
[3] J. Teissie, M. Prats, A. LeMassu, L. C. Stewart, and M. Kates, Biochemistry **29**, 59 (1990).
[4] M. Pasenkiewicz-Gierula, Y. Takaoka, H. Miyagawa, K. Kitamura, and A. Kusumi, Biophysik **76**, 1228 (1999).
[5] B. Bagchi, Chem. Rev. (Washington, D.C.) **105**, 3197 (2005).
[6] C. P. Swaminathan, N. Surolia, and A. Surolia, J. Am. Chem. Soc. **120**, 5153 (1998).
[7] B. Jayaram and T. Jain, Annu. Rev. Biophys. Biomol. Struct. **33**, 343 (2004).
[8] N. Nandi and B. Bagchi, J. Phys. Chem. B **101**, 10954 (1997).
[9] J. Milhaud, Biochim. Biophys. Acta **1663**, 19 (2004).
[10] E. A. Disalvo, F. Lairion, F. Martini, E. Tymczyszyn, M. Frías, H. Almaleck, and G. J. Gordillo, Biochim. Biophys. Acta **1778**, 2655 (2008).
[11] W. Zhao, D. E. Moilanen, E. E. Fenn, and M. D. Fayer, J. Am. Chem. Soc. **130**, 13927 (2008).
[12] J. F. Nagle and S. Tristram-Nagle, Biochim. Biophys. Acta **1469**, 159 (2000).
[13] S. Tristram-Nagle and J. F. Nagle, Chem. Phys. Lipids **127**, 3 (2004).
[14] I. R. Piletic, D. E. Moilanen, D. B. Spry, N. E. Levinger, and M. D. Fayer, J. Phys. Chem. A **110**, 4585 (2006).
[15] D. E. Moilanen, D. B. Spry, N. E. Levinger, and M. D. Fayer, J. Am. Chem. Soc. **129**, 14311 (2007).
[16] K. V. Damodaran and J. K. M. Merz, Langmuir **9**, 1179 (1993).
[17] M. Pasenkiewicz-Gierula, Y. Takaoka, H. Miyagawa, K. Kitamura, and A. Kusumi, J. Phys. Chem. A **101**, 5596 (1997).
[18] C. F. Lopez, S. O. Nielsen, M. L. Klein, and P. B. Moore, J. Phys. Chem. B **108**, 6603 (2004).
[19] T. Róg, K. Murzyn, and M. Pasenkiewicz-Gierula, Chem. Phys. Lett. **352**, 323 (2002).
[20] S. Y. Bhide and M. L. Berkowitz, J. Chem. Phys. **125**, 094713 (2006).
[21] Z. Zhang and M. L. Berkowitz, J. Phys. Chem. B **113**, 7676 (2009).
[22] J. Åqvist, C. Medina, and J. E. Samuelsson, Protein Eng. **7**, 385 (1994).
[23] Y. Y. Sham, Z. T. Chu, H. Tao, and A. Warshel, Proteins **39**, 393 (2000).
[24] F. S. Lee, Z.-T. Chu, M. B. Bolger, and A. Warshel, Protein Eng. **5**, 215 (1992).
[25] J. Florián and A. Warshel, J. Phys. Chem. B **103**, 10282 (1999).
[26] B. Jana, S. Pal, P. K. Maiti, S.-T. Lin, J. T. Hynes, and B. Bagchi, J. Phys. Chem. B **110**, 19611 (2006).
[27] S.-T. Lin, M. Blanco, and W. A. Goddard, J. Chem. Phys. **119**, 11792 (2003).
[28] S.-T. Lin, P. K. Maiti, and W. A. Goddard, J. Phys. Chem. B **114**, 8191 (2010).
[29] S.-T. Lin, P. K. Maiti, and W. A. Goddard, J. Phys. Chem. B **109**, 8663 (2005).
[30] P. K. Maiti and B. Bagchi, Nano Lett. **6**, 2478 (2006).
[31] L. Wang, R. A. Friesner, and B. J. Berne, J. Chem. Theory Comput. **5**, 1462 (2009).
[32] R. H. Henchman, J. Chem. Phys. **126**, 064504 (2007).
[33] M. Klefas-Stennett and R. H. Henchman, J. Phys. Chem. B **112**, 9769 (2008).
[34] J. Zielkiewicz, J. Phys. Chem. B **112**, 7810 (2008).
[35] M. A. R. Sharma and C. Chakravary, Mol. Phys. **106**, 1925 (2008).
[36] K. Murzyn, W. Zhao, M. Karttunen, M. Kurdziel, and T. Róg, BioInterphases **1**, 98 (2006).
[37] G. Garberoglio, M. Sega, and R. Vallauri, J. Chem. Phys. **126**, 125103 (2007).
[38] See topologies for http://moose.bio.ucalgary.ca/index.php?page=Structures_and_Topologies.
[39] D. van der Spoel, E. Lindahl, B. Hess, A. R. van Buuren, E. Apol, P. J. Meulenhoff, D. P. Tieleman, A. L. T. M. Sijbers, K. A. Feenstra, R. van Drunen, and H. J. C. Berendsen, GROMACS User Manual, version 3.3 (2006).
[40] H. Berendsen, J. P. M. Postma, W. F. van Gunsteren, and J. Hermans, *Intermolecular Forces* edited by B. Pullman (Reidel, Dordrecht, 1981).
[41] P. Mark and L. Nilsson, J. Phys. Chem. A **105**, 9954 (2001).
[42] H. J. C. Berendsen, J. P. M. Postma, W. F. van Gunsteren, A. Dinola, and J. R. Hak, J. Chem. Phys. **81**, 3684 (1984).
[43] H. J. C. Berendsen, D. van der Spoel, and R. van Drunen, Comput. Phys. Commun. **91**, 43 (1995).
[44] E. Lindahl, B. Hess, and D. van der Spoel, J. Mol. Model. **7**, 306 (2001).
[45] K. V. Damodaran and K. M. Merz, Biophys. J. **66**, 1076 (1994).
[46] C. Rocchi, A. R. Bizzarri, and S. Cannistraro, , Phys. Rev. E **57**, 3315 (1998).
[47] D. Laage and J. T. Hynes, Science **311**, 832 (2006).
[48] D. Laage and J. T. Hynes, Chem. Phys. Lett. **433**, 80 (2006).
[49] D. Laage and J. T. Hynes, Proc. Natl. Acad. Sci. U.S.A. **104**, 11167 (2007).
[50] D. Laage and J. T. Hynes, J. Phys. Chem. B **112**, 14230 (2008).
[51] B. Jana, S. Pal, and B. Bagchi, J. Phys. Chem. B **112**, 9112 (2008).
[52] N. Levinger and L. Swafford, Annu. Rev. Phys. Chem. **60**, 385 (2009).
[53] D. E. Moilanen, E. E. Fenn, D. Wong, and M. D. Fayer, J. Chem. Phys. **131**, 014704 (2009).
[54] D. E. Moilanen, E. E. Fenn, D. Wong, and M. D. Fayer, J. Phys. Chem. B **113**, 8560 (2009).
[55] R. L. A. Timmer and H. J. Bakker, J. Phys. Chem. A **113**, 6104 (2009).
[56] J. Chowdhary and B. M. Ladanyi, J. Phys. Chem. B **112**, 6259 (2008).
[57] D. Laage, J. Phys. Chem. B **113**, 2684 (2009).
[58] D. Laage and H. T. Hynes, J. Phys. Chem. B **112**, 7697 (2008).
[59] K. Winkler, J. Lindner, H. Bürsing, and P. Vöhringer, J. Chem. Phys. **113**, 4674 (2000).
[60] H. Cang, V. Novikov, and M. Fayer, J. Chem. Phys. **118**, 2800 (2003).

[61] G. R. Fleming, *Chemical Applications of Ultrafast Spectroscopy* (Oxford University Press, New York, 1986).
[62] H. S. Tan, I. R. Piletic, and M. D. Fayer, J. Chem. Phys. **122**, 174501 (2005).
[63] G. Lipari and A. Szabo, Biophys. J. **30**, 489 (1980).
[64] C. C. Wang and R. Pecora, J. Chem. Phys. **72**, 5333 (1980).
[65] B. Mukherjee, P. K. Maiti, C. Dasgupta, and A. K. Sood, ACS Nano **2**, 1189 (2008).
[66] B. J. Berne and R. Pecora, *Dynamic Light Scattering with Applications to Chemistry, Biology and Physics* (Wiley, New York, 1976).
[67] S. Woutersen, U. Emmerich, and H. J. Bakker, Science **278**, 658 (1997).
[68] B. Mukherjee, P. K. Maiti, C. Dasgupta, and A. K. Sood, J. Phys. Chem. B **113**, 10322 (2009).
[69] B. Mukherjee, P. K. Maiti, C. Dasgupta, and A. K. Sood, J. Nanosci. Nanotechnol. **9**, 5303 (2009).
[70] K. J. Tielrooij, D. Paparo, L. Piatkowski, H. J. Bakker, and M. Bonn, Biophys. J. **97**, 2484 (2009).
[71] M. G. Mazza, N. Giovambattista, F. W. Starr, and H. E. Stanley, Phys. Rev. Lett. **96**, 057803 (2006).
[72] N. F. Carnahan and K. E. Starling, J. Chem. Phys. **53**, 600 (1970).
[73] A. A. McQuarrie, *Statistical Mechanics* (Harper and Row, New York, 1976).
[74] H. S. Frank and M. W. Evans, J. Chem. Phys. **13**, 507 (1945).
[75] Y. Rezus and H. J. Bakker, Phys. Rev. Lett. **99**, 148301 (2007).
[76] C. L. Dias, T. Ala-Nissila, J. Wong-ekkabut, I. Vattulainen, M. Grant, and M. Karttunen, Cryobiology **60**, 91 (2010).